The Role of Duty Cycle in a Three Cell Central Pattern Generator

Jeremy Wojcik, Robert Clewley and Andrey Shilnikov

Abstract We describe a novel computational approach to reduce detailed models of central pattern generation to an equationless mapping that can be studied geometrically. Changes in model parameters, coupling properties, or external inputs produce qualitative changes in the mapping. These changes uncover possible biophysical mechanisms for control and modulation of rhythmic activity. Our analysis does not require knowledge of the equations that model the system, and so provides a powerful new approach to studying detailed models, applicable to a variety of biological phenomena beyond motor control. We demonstrate our technique on a motif of three reciprocally inhibitory cells that is able to produce multiple patterns of bursting rhythms. In particular, we examine the qualitative geometric structure of two-dimensional maps for phase lag between the cells.

1 Introduction

A central pattern generator (CPG) is a neural microcircuit comprised of cells whose synergetic interactions, without a sensory input, can produce rhythmic bursting patterns that determine motor behaviors of an animal, such as heart beat, respiration, and locomotion [1, 2]. A multifunctional CPG can exhibit distinct rhythmic behaviors depending on input conditions: for example, switching between trot and gallop gaits in many mammals [3] or between swimming and crawling in leeches [4, 5]. Although

J. Wojcik (✉) · R. Clewley · A. Shilnikov
Neuroscience Institute and Department of Mathematics and Statistics,
Georgia State University, PO Box 5030, Atlanta, GA 30303, USA
e-mail: jwojcik1@gsu.edu

R. Clewley
e-mail: rclewley@gsu.edu

A. Shilnikov
e-mail: ashilnikov@gsu.edu

such circuits are mostly hypothetical in the central nervous system of mammals, they have been located in many fish and invertebrates and in the spinal cord or peripheral nervous systems of mammals.

Switching between motor rhythms in a multifunctional CPG is attributed to switching between corresponding oscillatory attractors [5]. A key scientific issue is how modulation and control can switch the system between states, and how the CPG achieves robustness to noise and heterogeneity. Theoretically, the problem is therefore how to obtain parsimonious answers to the scientific questions through mathematical analysis and simulation of these models. A common approach has been to first reduce each neuron's activity to a one- or two-dimensional return map using, for example, phase resetting techniques, and then to compose these maps to form an approximate representation of the cycle-to-cycle network activity [6, 7]. Instead, we directly analyze a single return map induced by the full dynamics of a biophysical network CPG model. This map will be defined qualitatively through numerical simulations and does not require knowledge of explicit phase equations for the underlying network model. This makes our technique applicable to a wide range of detailed (high-dimensional) models of rhythmic activity in biological networks, especially those that are not easily reduced to low-dimensional systems of equations by explicit means.

Elemental circuit configurations for CPG models are often reduced to three oscillators but their components are typically anatomically and physiologically diverse [8–11]. We consider a model of endogenously bursting neurons coupled in a ring [12] using fast reciprocal synaptic inhibition modeled by fast threshold modulation [13]. The neurons are 3-dimensional reduced models of leech heart interneurons, as defined in ref. [14]. We demonstrate that the duty cycle of bursting, the fraction of the burst period in which the cell bursts, is a physiologically relevant order parameter that can be used to control switching between outcomes.

2 Qualitative Analysis of Phase-Lag Maps

We examine polyrhythmic outcomes of the motif for *short* ($\sim$20 %), *medium* ($\sim$50 %), and *long* ($\sim$80 %) bursting duty cycles. For this we computationally derive return maps for phase lags $\Delta\phi_{21}$ and $\Delta\phi_{31}$ between burst onsets in cell 2 (green) and cell 3 (red) relative to the reference cell 1 (blue) (Fig. 1). As the period of network oscillation changes through time, we define the phase between cells to be relative to the time interval between which the voltage V_1 of cell 1 increases through a threshold of -40 mV. We define $\Delta\phi_{i1}^{(n)} \in [0, 1)$ as the phase lag between the nth consecutive burst onsets in cells 1 and i. As the network evolves from an initial state, the relative phases of each oscillator on each subsequent cycle n generate a sequence $\{\Delta\phi_{31}^{(n)}, \Delta\phi_{21}^{(n)}\}$, which we plot within the unit square; for convenience the iterates are joined with lines to preserve cycle ordering in the phase lag maps (Figs. 2, 3). Thus, the original, continuous-time 9D system is reduced to a 2D stroboscopic
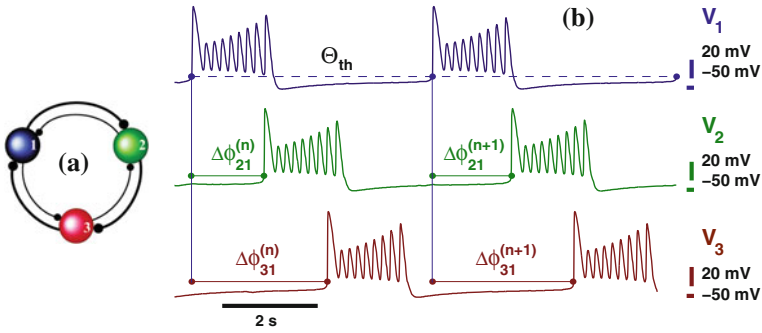
Fig. 1 Voltage traces: the phase (mod 1) of reference cell 1 (*blue*) is reset when V_1 reaches $\Theta_{th} = -40$ mV. The time between burst onsets in cell 2 (*green*) and 3 (*red*) determine a sequence of phase lags $\{\Delta\phi_{21}^{(n)}, \Delta\phi_{31}^{(n)}\}$ normalized to the varying recurrence times of cell 1
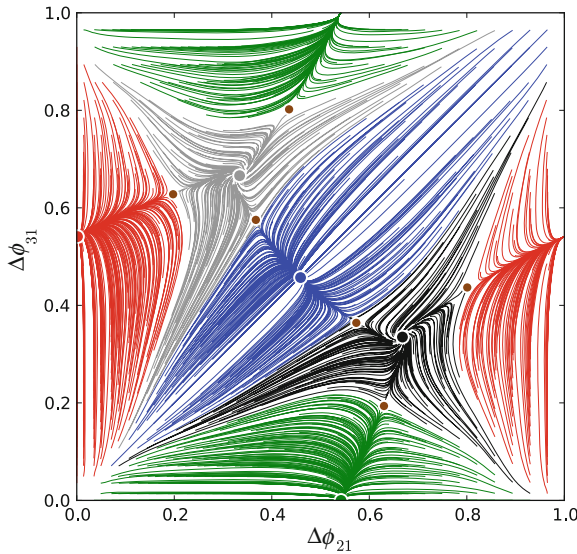
Fig. 2 Phase-lag map for the homogeneous, medium bursting motif at $V_{K2}^{shift} = -21.0$ mV, showing five phase-locked (fixed point) attractors: *red* at $\sim \left(0, \frac{1}{2}\right)$, *green* $\left(\frac{1}{2}, 0\right)$, *blue* $\left(\frac{1}{2}, \frac{1}{2}\right)$, *black* $\left(\frac{2}{3}, \frac{1}{3}\right)$ and *gray* $\left(\frac{1}{3}, \frac{2}{3}\right)$, whose basins are separated by six saddles (*brown dots*)

return map for the phase lags defined on a torus $[0, 1) \times [0, 1)$, with $\Delta\phi_{i1}$ mod 1. The maps are not derived as explicit equations, but instead are tabulated on a 40×40 (or more) grid of initial points whose iterates comprehensively reveal the underlying vector field. We then study the geometric properties of the maps. In particular, we can locate equilibrium points of the maps, which we refer to as fixed points (FPs). We evaluate the stability of these objects and characterize bifurcations by using the methods of the qualitative theory of dynamical systems.

Figure 2 shows the $(\Delta\phi_{31}, \Delta\phi_{21})$ phase-lag map for the homogeneous, medium bursting motif when $V_{K2}^{shift} = -21.0\,\mathrm{mV}$. The map possesses five stable FPs (color-coded dots) corresponding to the coexisting phase-locked bursting patterns: red at $\left((\Delta\phi_{21} \approx 0, \Delta\phi_{31} \approx \frac{1}{2})\right)$, green $\left(\frac{1}{2}, 0\right)$, blue $\left(\frac{1}{2}, \frac{1}{2}\right)$, black $\left(\frac{2}{3}, \frac{1}{3}\right)$ and gray $\left(\frac{1}{3}, \frac{2}{3}\right)$. The attraction basins of these points are divided by separatrices (incoming and outgoing sets) of six saddle points (brown dots). The saddles separate the basins of attraction of the 5 fixed points which correspond to phase locked states.

The outcome of the homogeneous motif depends on the initial phase distributions of the cells. When the cells are about to burst together, their initial phases are near the origin in the phase plane. In this case, any of the five rhythmic pattern outcomes has a chance of occurring (Fig. 2). Each rhythm is robust, so well chosen perturbations are needed to switch the motif between rhythms. An efficient and easy way to perturb an inhibitory motif is to apply an appropriately-timed hyperpolarizing pulse to the targeted cell [12, 15]. Figure 4 demonstrates the approach for the homogeneous motif. The phase-lag maps create a guide for where and how long a hyperpolarizing pulse is needed to switch between rhythms. For example, if we begin at the FP $\left(\frac{1}{2}, \frac{1}{2}\right)$ and perturb cell 2 (green) we change the phase-lags $\Delta\phi_{21}$ and $\Delta\phi_{31}$. This changes the position on the phase lag diagram and moves the phase point into the basin of attraction of another rhythm, as in Fig. 1.
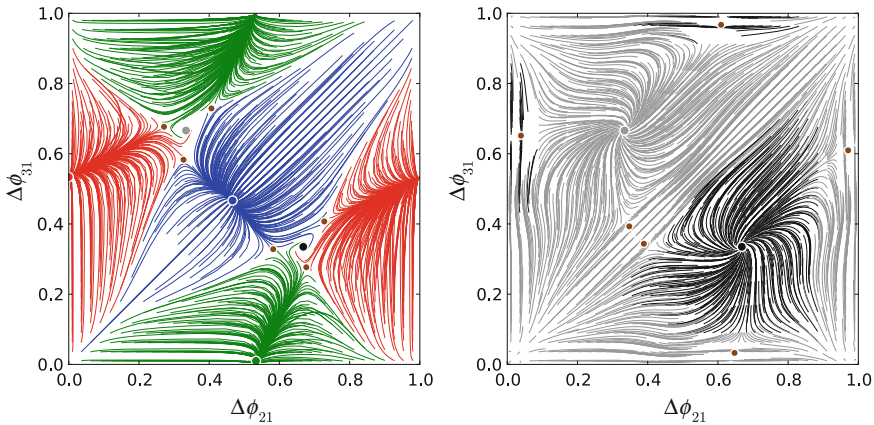
Fig. 3 Homogeneous phase-lag mapping for $V_{K2}^{shift} = -18.95\,\mathrm{mV}$ motif at $V_{K2}^{shift} = -18.95\,\mathrm{mV}$, showing three attractors (*blue, red*, and *green dots*). Each corresponds to an anti-phase rhythm where one cell bursts solo followed by synchronized bursts in the other two cells. The fixed points for counter-clockwise and clockwise traveling waves (*black dots*) are unstable. *Right* Phase-lag map for the homogeneous, long bursting motif at $V_{K2}^{shift} = -22.5\,\mathrm{mV}$, revealing two equally dominant rhythmic attractors: at $\left(\frac{1}{3}, \frac{2}{3}\right)$ and at $\left(\frac{2}{3}, \frac{1}{3}\right)$
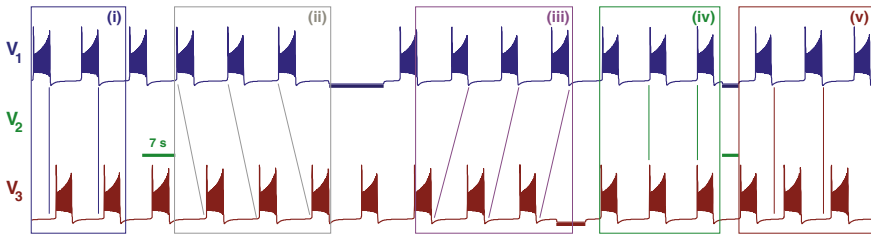
Fig. 4 Five types of robust bursting rhythms in the medium-length bursting motif, using $g_{\text{syn}} = 5 \cdot 10^{-3}$ (increased from its nominal value to illustrate stable states without long transients). Appropriately-timed inhibitory pulses (horizontal bars) temporarily suppress the targeted cells and switch between the rhythms. Episode (*i*) shows the $\left(\frac{1}{2}, \frac{1}{2}\right)$ FP interrupted by a pulse to cell 2. On release of cell 2 from suppression, the clockwise $\left(\frac{1}{3}, \frac{2}{3}\right)$ FP is observed. After cell 1 is temporarily suppressed, the counter-clockwise $\left(\frac{2}{3}, \frac{1}{3}\right)$ FP is observed in episode (*iii*). A pulse releasing cell 3 from inhibition then makes cell 2 lead in the $\left(0, \frac{1}{2}\right)$ rhythm of episode (*iv*). After cells 1 and 2 have been simultaneously hyperpolarized, cell 3 leads the motif in the $\left(\frac{1}{2}, 0\right)$ in the last episode (*v*) of the voltage trace

3 Duty Cycle is an Order Parameter of the Network

The duty cycle (DC) of bursting oscillations is the fraction of the burst period in which the cell is spiking (Fig. 1), and is a property known to affect the synchronization properties of coupled bursters [15]. DC can be measured experimentally from voltage traces in neural dynamics. In this study, we control DC through the intrinsic parameter $V_{\text{K2}}^{\text{shift}}$, which measures the deviation from the experimentally identified voltage value at which the slow K^+ current is half-activated [14]. DC depends monotonically on $V_{\text{K2}}^{\text{shift}}$. As the activation kinetics of this current are shifted to depolarized voltages, the cells produce first short, then medium, and then long burst trains before transitioning to continuous spiking. We consider weak inhibitory coupling determined by the maximal conductance g_{syn}, which is set at $5 \cdot 10^{-4}$ nS in the homogeneous case.

Comparison of the maps for the homogeneous motifs in cases of medium (Fig. 2), short (Fig. 3, left) and long (Fig. 3, right) bursting demonstrates that the DC is an order parameter for such configurations. As such, short bursting (DC $\sim 20\%$) makes both traveling waves impossible because the corresponding FPs exist but are unstable. In contrast, for long bursting (DC $\sim 80\%$), these patterns equally dominate the dynamics by narrowing the attractor basin of the other FPs—shrinking the range of phases that can lead to alternative patterns.

4 Summary

In this work we presented a simple network motif of three bursting cells reciprocally coupled by fast inhibitory synapses in a ring. We showed that the model can generate multiple, coexisting rhythms, selected by the initial conditions of the

cells. We characterized the essential temporal properties of the coupled system by measuring just two differences ("lags") in the phase between the three oscillators along simulated orbits. By systematic variation of the initial conditions, the computational exploration of the possible rhythmic outcomes led to a reduction of the original 9D system of differential equations to a graphical and equationless representation of the 2D mapping of cycle-to-cycle phase lags. Crucially, a feature of this reduction is that explicit equations were replaced by a qualitative portrait of the maps. Nonetheless, the geometric properties of the maps, and how they change as model parameters are varied, can be understood through standard qualitative techniques of dynamical systems theory. In particular, the rhythmic patterns of the motif correspond to fixed and periodic attractors of the maps. The basins of attraction for the rhythms are separated by phase thresholds known as saddles.

The power of our technique is that it avoids the need for equations, and as such makes few assumptions about the nature of the models of the coupled oscillators making up the motif or their detailed form of coupling. For instance, the models may be high-dimensional and possess multiple time scales. In order to define the phase lags, we only assume that the cells burst regularly. In principle, our technique can be generalized to a larger number of cells. Problems of human visualization of higher-dimensional phase-lag maps notwithstanding, the concepts of fixed points and periodic orbits carry through to higher dimensions.

We discovered that the primary "order parameter" determining the pattern outcomes is the duty cycle of bursting: short bursting promotes anti-phase rhythms, while long bursts will self-arrange into one of two traveling wave patterns typical of unidirectionally-coupled inhibitory rings. The dynamics of the motif with medium-length duty cycle is richer due to the existence of five competing rhythmic outcomes. We therefore hypothesize a possible biophysical control mechanism for switching between CPG patterns: common inhibition or excitation to the circuit, which varies the duty cycle of all cells simultaneously. For complete details see [16, 17] and references therein.

References

1. E. Marder, R.L. Calabrese, Principles of rhythmic motor pattern generation. Physiol. Rev. **76**, 687–717 (1996)
2. F. Skinner, N. Kopell, E. Marder, Mechanisms for oscillation and frequency control in networks of mutually inhibitory relaxation oscillators. J. Comput. Neurosci. **1**, 69–97 (1994)
3. A. Selverston, *Model Neural Networks and Behavior* (Plenum Press, New York, 1985)
4. K.L. Briggman, W.B. Kristan, Multifunctional pattern generating circuits. Annu. Rev. Neurosci. **31**, 271–294 (2008)
5. W.B. Kristan, R.L. Calabrese, W.O. Friesen, Neuronal basis of leech behaviors. Prog. Neurobiol. **76**, 279–327 (2005)
6. C.C. Canavier, D.A. Baxter, J.W. Clark, J.H. Byrne, Control of multistability in ring circuits of oscillators. Biol. Cybern. **80**, 87–102 (1999)
7. G.B. Ermentrout, K. Kopell, Fine structure of neural spiking and synchronization in the presence of conduction delays. Proc. Natl. Acad. Sci. USA **95**, 1259–1264 (1998)

8. R. Milo, et al., Science **298**, 824–827 (2002)
9. A. Prinz, D. Bucher, E. Marder, Similar network activity from disparate circuit parameters. Nat. Neurosci. **7**(12), 1345–1352 (2004)
10. M.I. Rabinovich, P. Varona, A.I. Selverston, H.D. Abarbanel, Dynamical principles in neuroscience. Rev. Modern. Phys. **78**(4), 1213–1265 (2006)
11. O. Sporns, R. Kötter, Motifs in brain networks. PLoS Biol. **2**(11), 1910–1918 (2004)
12. A. Shilnikov, R. Gordon, I. Belykh, Polyrhythmic synchronization in bursting network motif. Chaos **18**, 037120 (2008)
13. N. Kopell, D. Somers, Rapid synchronization through fast threshold modulation. Biol. Cybern. **68**(5), 393–407 (1993)
14. A. Shilnikov, G. Cymbalyuk, Transition between tonic-spiking and bursting in a neuron model via the blue-sky catastrophe. Phys. Rev. Lett. **94**, 048101-4 (2005)
15. I. Belykh, A. Shilnikov, When weak inhibition synchronizes strongly desynchronizing networks of bursting neurons. Phys. Rev. Lett. **101**, 078102-4 (2008)
16. J. Wojcik, A.L. Shilnikov, Order parameter for bursting polyrhythms in multifunctional central pattern generators. Phys. Rev. E **83**, 056209-6 (2011)
17. J. Wojcik, Neural Cartography: Computer Assisted Poincaré Return Mappings for Biological Oscillations Mathematics Dissertations. Paper 10. http://digitalarchive.gsu.edu/math_diss/10 (2012)